Reprinted from *Analysis Methods for Multi-Spacecraft Data*Götz Paschmann and Patrick W. Daly (Eds.),
ISSI Scientific Report SR-001 (Electronic edition 1.1)
© 1998, 2000 ISSI/ESA

# **— 16 —**

# **Accuracy of Current Density Determination**

#### PATRICK ROBERT

Centre National de la Recherche Scientifique, Vélizy, France

## MALCOLM W. DUNLOP

Imperial College of Science, Technology and Medicine London, United Kingdom

### ALAIN ROUX AND GERARD CHANTEUR

Centre National de la Recherche Scientifique, Vélizy, France

# 16.1 Introduction

The four Cluster spacecraft will enable simultaneous measurements of the vector magnetic field at the vertices of a tetrahedron. Methods for analysing such data include: a contour integral method for determining the electric current density (from  $\nabla \times \boldsymbol{B}$ ) in fields varying on scales relatively large compared to the spacecraft separations, and which was coined the "curlometer" technique; a wave telescope technique which is most reliable where the field scale variations are comparable to the spacecraft separations; and a discontinuity analysis technique for cases where the field scale variations are much shorter than the spacecraft separations. Note that the Curlometer also provides an estimate of  $\nabla \cdot \boldsymbol{B}$  via Gauss's Theorem. The finite difference equations at the core of the curlometer technique can also be derived and efficiently solved by making use of barycentric coordinates. A collection of methods based on barycentric coordinates are fully described in Chapter 14. In the linear approximation, the barycentric estimates for  $\nabla \times \boldsymbol{B}$  and  $\nabla \cdot \boldsymbol{B}$  are identical to those defined by contour integrals (as they should be for mathematical consistency).

For this reason, both forms are used here as a matter of mathematical convenience: to employ the computational efficiency of the barycentric equations for the statistical analysis, for instance. The resulting estimates of J and the divergence of B are subject to errors of which there are basically three types. The first relates to measurement uncertainties in B, and in the spatial configuration of the four spacecraft. The second relates to the linear interpolation which is made between the various measurement points. The third relates to the simultaneity of the measurements. Sections 14.3 and 14.4 present theoretical investigations of the first and second types of errors respectively.

The influence of these errors on the accuracy of the estimate of J or  $\nabla \cdot B$  is strongly related to the shape of the tetrahedron but also to the magnetic structure present. This, of course, is not known (at least explicitly) for measured data. Since the shape of this tetrahedron evolves along the mean trajectory of the 4 spacecraft, it is particularly important to

study the influence of the shape of the tetrahedron on the accuracy of the estimate of the current density.

First of all, we identify the general basis for the curlometer method. We briefly explore the effect of magnetic structure on the quality of the estimate of J, particularly highlighting the possible effect of anisotropic structure on sampling, and set this in the Cluster context.

Then, using randomly simulated configurations for the case of a particular isotropic magnetic structure, we discuss the following quantitative questions, in some detail: (i) what parameters we have to use to characterise the shape of a given tetrahedron? (ii) what is the relation between the geometrical shape of the tetrahedron and the accuracy of the determination of J via the estimate of  $\nabla \times B$ ? (iii) can  $\nabla \cdot B$  be used as an estimate of the error  $\Delta J$ , as opposed to its use as a general indicator of physical coverage<sup>1</sup>? and (iv) when the tetrahedron is relatively flat, is there a relation between the accuracy of the determination of J and the orientation of the current with respect to the orientation of the tetrahedron? These questions are studied with the help of a numerical simulation based on a large number of possible tetrahedra and a model for the current structure.

# 16.2 The Curlometer Technique

## 16.2.1 Background

Use of the magnetic field alone requires the electric current density to be estimated from Ampère's law, which is physically valid over the dynamic range of dc magnetometer measurements. By treating this current as constant over the tetrahedral volume formed by the four spacecraft, a difference estimate of  $\nabla \times \boldsymbol{B}$  can be made. This estimate forms the basis of the curlometer analysis technique. In reality, the current will always vary to some degree over the tetrahedron and the best (a priori) knowledge of this lies in estimating  $\nabla \cdot \boldsymbol{B}$  under the same assumptions. Because of the solenoidality of the magnetic field ( $\nabla \cdot \boldsymbol{B} = 0$ ), any non-zero result arising from this estimate of  $\nabla \cdot \boldsymbol{B}$  arises from the neglected nonlinear gradients in  $\boldsymbol{B}$  (assuming that the error measurement is weak by respect to the error due to the nonlinear gradients). These are of the same order as the second order terms in  $\nabla \times \boldsymbol{B}$ , dropped by differencing (see below). This quantity only partly reflects the physical error, arising from the coverage of the magnetic structure achieved by the spacecraft tetrahedron, in the context of the gradients contributing to  $\nabla \cdot \boldsymbol{B}$ . The gradient of  $\boldsymbol{B}$  and the nonlinear contributions for  $\nabla \times \boldsymbol{B}$ , in particular, are not checked explicitly. The use of the estimate of  $\nabla \cdot \boldsymbol{B}$  serves in this method as a quality indicator only.

During the development of the method the suitability of  $\nabla \cdot \boldsymbol{B}$  as a measure of the physical uncertainty was extensively tested. It was concluded that for some structures  $\nabla \cdot \boldsymbol{B}$  does not necessarily form a particularly good estimate of the error in  $\boldsymbol{J}$ . In particular, for the case of a current tube, if statistically  $\nabla \cdot \boldsymbol{B}$  and  $\Delta \boldsymbol{J}$  show the same variation, there is no point to point correspondence (see Section 16.4.3). This has been also suggested by comparisons of the  $\boldsymbol{J}$  vector of the Tsyganenko-87 magnetic field model deduced from the Cluster tetrahedron by the barycentric method with the  $\boldsymbol{J}$  vector deduced by a finite difference method on an arbitrary small scale.

<sup>&</sup>lt;sup>1</sup>What is called here "physical coverage" and "nonlinear contributions" is related to the errors of truncation (see section 14.4).

For *in situ* analysis, the significance of  $\nabla \cdot \boldsymbol{B}$  should therefore be quantified in terms of the interpretation of the data being made (see Section 16.2.3), i.e., in terms of the properties of different model structures being implied. Nevertheless, in many instances  $\nabla \cdot \boldsymbol{B}/|\nabla \times \boldsymbol{B}|$  can be used to discuss the quality of the current estimate.

The difference approximation leads via the integral form of Ampère's law to:

$$\mu_0 \boldsymbol{J}_{\text{av}} \cdot (\boldsymbol{r}_{1\alpha} \times \boldsymbol{r}_{1\beta}) = \Delta \boldsymbol{B}_{1\alpha} \cdot \boldsymbol{r}_{1\beta} - \Delta \boldsymbol{B}_{1\beta} \cdot \boldsymbol{r}_{1\alpha}$$
 (16.1)

$$\langle \nabla \cdot \boldsymbol{B} \rangle_{\text{av}} | \boldsymbol{r}_{1\alpha} \cdot (\boldsymbol{r}_{1\beta} \times \boldsymbol{r}_{1\gamma}) | = | \sum_{\text{cyclic}} \Delta \boldsymbol{B}_{1\alpha} \cdot (\boldsymbol{r}_{1\beta} \times \boldsymbol{r}_{1\gamma}) |$$
 (16.2)

where we have chosen to define differences between spacecraft to be relative to spacecraft 1;  $\alpha$ ,  $\beta$ ,  $\gamma$  = 2, 3 and 4 are indices referring to the apexes of the tetrahedron.  $J_{av}$  represents the measured mean current over the tetrahedron volume (= $J^{\text{estimated}}$  in Section 16.3), and  $(\nabla \cdot \boldsymbol{B})_{av}$  is the differential estimate of  $\nabla \cdot \boldsymbol{B}$  for the tetrahedron.  $\boldsymbol{r}_{1\alpha}$  and  $\Delta \boldsymbol{B}_{1\alpha}$  represent the separation vectors and field differences between respective spacecraft. These equations give the current normal to each face of the tetrahedron and therefore represent a coordinate independent, natural expression of the current relative to the tetrahedral geometry and orientation. As such, they immediately give a reflection of the physical coverage of the magnetic structure sampled by the spacecraft array (note that the fourth face, not involving spacecraft 1, forms a redundant estimate, but can be obtained by changing the reference spacecraft). If independent reference components of  $J_{\rm av}$  are required, these can, of course, be extracted by a further transformation, or by direct calculation, using the cartesian, differential form of the equations, for example, and also with an equivalent coordinate-independent formalism, employing barycentric coordinates. In Chapter 14 the use of the barycentric method is completely described, including the extraction of the difference estimates for  $\nabla \times \mathbf{B}$  and  $\nabla \cdot \mathbf{B}$ .

Apart from the physical error (lack of accurate coverage by the spacecraft configuration), the change in the current estimate,  $\delta J$ , due to errors in the spacecraft separations and in the magnetic field values measured at each spacecraft, can be estimated through an error analysis of equation 16.1. Other sources of error, such as timing errors, are usually relatively unimportant or are considered part of the field error. The relative measurement error  $\delta J/|J_{\rm av}|$  is used as the prime monitor of measurement performance in  $J_{\rm av}$ . It is useful for understanding the variability found for  $\delta J$  to express this conceptually as follows:

$$\frac{\delta J}{|J_{av}|} = F_B \frac{\delta B}{\Delta B} + F_S \frac{\delta r}{\Delta r} \tag{16.3}$$

where the field error and the separation error are taken as component independent for convenience of expression here.

In general, the form for  $\delta J$  is not separable, and is nonlinear. The above form, however, highlights the fact that the relative current error depends fundamentally on the relative measurement errors (in position and field), scaled by some factors,  $F_B$  and  $F_S$ , which depend on the field differences and the separation vectors (i.e., magnetic structure between the satellites and spacecraft configuration). Measurement and separation errors also contribute to  $\nabla \cdot \boldsymbol{B}$  itself and may be a large part of the estimate obtained *in situ*. Although for actual data this raises a further issue of interpretation of  $\nabla \cdot \boldsymbol{B}$ , for this work the use

of model (simulated) data and known uncertainties allows the effect to be considered separately.

It should be noted that the method used in this chapter is not trivially extendable to the case of more than 4 spacecraft. The basis for calculation of spatial gradients changes in that case since the nonlinear terms can then be checked directly (second order terms in the field differences can be determined), in principle, or the added redundancy with more than 4 points can be used to improve the physical estimates. Consideration of the significance of the measurement accuracy would guide how this information is best used.

## **16.2.2** Application: Cluster Context

The factors  $F_B$  and  $F_S$  above are of order unity in the "best case" situation of a regular tetrahedral configuration, sampling structures with spatial scales which are well matched by the overall scale of the tetrahedron. In general, these increase as the tetrahedron distorts, adversely affecting the contribution of these error sources, and typically,  $F_B$  and  $F_S$  are  $\sim 2-10$ , but this varies with magnetic structures also. Because of the critical nature of the error functions (for  $J_{av}$  but also for other combined parameters) and their sensitivity to spacecraft formation, the scientific performance of each measurement (not restricted to the magnetic field) will be highly constrained by orbital evolution. Typical values of the magnetic field measurement errors onboard Cluster are  $\sim 0.1\,\mathrm{nT}$  for typical magnetospheric magnetic fields along the Cluster orbit (up to  $\sim 1000\,\mathrm{nT}$ ). For the Cluster mission, a sequence of manoeuvres is anticipated which would modify the natural orbital evolution of the spacecraft configuration. Scientific analysis of a particular plasma environment is limited by the resulting scale size and shape of the spacecraft tetrahedron. A particular orbit phase will set both the configurational evolution over an orbit and the overall configuration scale in each magnetospheric region and this is depicted in Figure 16.1.

Two orbit phases are shown which have typically,  $1000\,\mathrm{km}$  separations (dayside) and  $1\,R_E$  separations (nightside), respectively. The insets in the dayside plot are enlargements of the projected configurations (×10). Very different evolution of the configuration is apparent which samples the model magnetic structure, taken from the Tsyganenko-87 field model, in a highly varied way. The curlometer method above allows the deformation over an orbit to be monitored in terms of its affect on the error functions for  $J_{\mathrm{av}}$ . This deformation is to the extent that such differential measurements would be prohibited for significant fractions of the orbit. Similarly, the effect on  $\nabla \cdot \boldsymbol{B}/|\nabla \times \boldsymbol{B}|$  can be monitored over the orbit. Each quantity can be used independently as an indicator of measurement performance: quality associated with measurement accuracy in the first case and quality of the physical coverage of gradients in the second case. Other quantities may have different regions of bad coverage.

In fact (see Figures 16.3 and 16.4), inspection of  $\nabla \cdot \boldsymbol{B}/|\nabla \times \boldsymbol{B}|$  and  $\delta J/|\boldsymbol{J}_{av}|$  reveals two facts. Firstly, small separations clearly achieve crudely better linearity estimates of spatial gradients, for some physical structure, since then the linear approximation is more accurate. Secondly, however, accuracy is limited by the relative measurement errors which become large at small separations because the absolute errors  $\delta \boldsymbol{B}$  and  $\delta \boldsymbol{r}$  are roughly constant. Thus, for a fixed orbital evolution, the overall quality represented by each parameter needs to be balanced: good linearity must still allow good relative measurement accuracy. This is represented in the Figure 16.2.

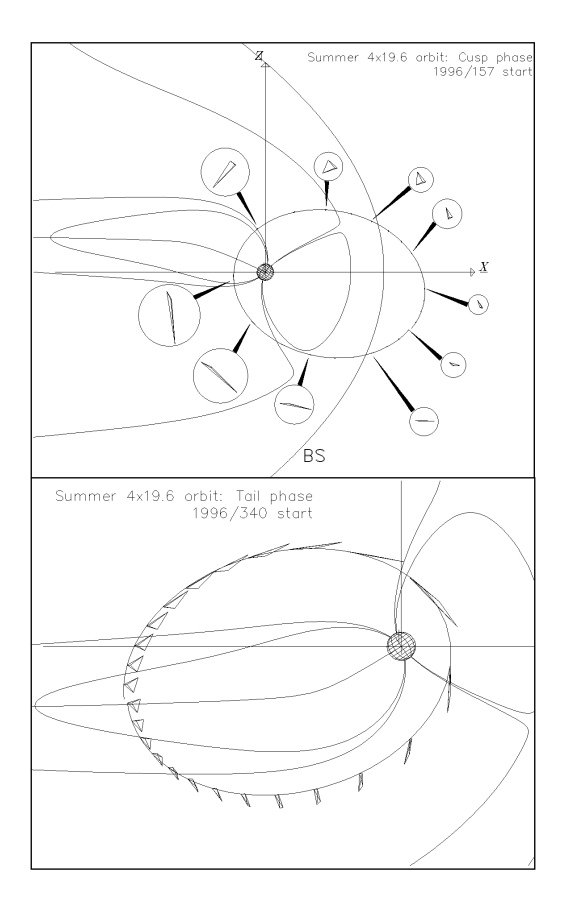


Figure 16.1: Dayside and nightside phases proposed for the first year of Cluster, showing the evolution of the spacecraft configuration.

Note that the curves shown are conceptual and, of course, change relative value depending upon the structure being sampled. The question is: what is achieved for a particular combined quantity (such as J) and for particular phenomena or regions of the orbit? For instance, the curves may cross at small or large separations and the quality of both the physical coverage and measurement may be high over a large range of scales, simultaneously. Not all magnetic structures are suitable for gradient analysis, of course, and in some instances other analysis techniques will be required for adequate performance.

A number of simple model structures have, in fact, been studied with simulated trajectories, having a range of spacecraft configurations, using the analysis tool described briefly in Section 16.2.3, below. It is clear from these studies that the characteristics contained in the magnetic structures (spatial variation), plays a critical role in the balance between the two conceptual curves shown above. The anisotropy and symmetry properties of the phenomena represented, changes the effect of the orientation of the spacecraft configuration relative to the structure, alters the contribution of the nonlinear variations to  $\nabla \cdot \boldsymbol{B}/|\nabla \times \boldsymbol{B}|$ , and, of course, affects the error functions defining  $\delta J/|\boldsymbol{J}_{av}|$ . The characteristic spatial scales of a phenomenon set the appropriate relative scales for the spacecraft

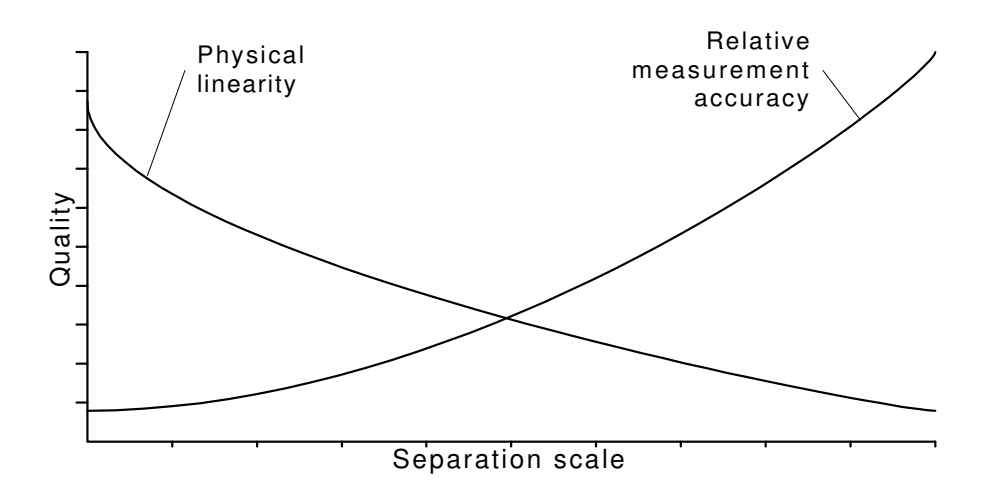


Figure 16.2: Comparison of quality trends with the overall scale of the spacecraft configuration.

configuration (a key factor in defining the Cluster orbital phases). This sensitivity to magnetic structure is often complex since sampled events may exhibit a number of properties (waves on boundaries, flux ropes, etc.) and is beyond the scope of the present chapter. In the second part of this chapter, rather, a detailed study of configuration dependence is discussed for a particular, important magnetic structure.

Over an orbit containing some configurational evolution, the two quality indicators  $(\nabla \cdot \boldsymbol{B}/|\nabla \times \boldsymbol{B}| \text{ and } \delta J/|\boldsymbol{J}_{av}|)$  will exhibit individual error profiles, highly sensitive to both the characteristic anisotropy and spatial scales of the magnetic structure sampled and the geometry, relative orientation and relative size of the spacecraft configuration. Figures 16.3 and 16.4 show examples of these sensitivities for the case of anticipated Cluster situations in order to give a brief indication of the key results.

Referring back to the dayside orientation for the orbit shown in Figure 16.3, it should be noted that many other evolutions will result for different starting configurations (here chosen to be a regular tetrahedron at the northern cusp), but that the overall scale, within this evolution, is set by the scale of the starting configuration.

Profiles for the two parameters are shown for two, similar choices for dayside phases in the Figure 16.3. This plot shows variation against the true anomaly around the orbit, with the evolution outside the magnetopause not shown and where the field is sampled at the times over the orbit for each tetrahedral position. A nominal separation error of 5 km and a measurement error of 0.1 nT in the field have been assumed (no component error dependence is monitored for simplicity). The parameters monitor poor quality (large values here) when error contributions are high. Features in the trends arise from a combination of the effect of local magnetic structure, the relative separation scale and the degree of tetrahedral distortion. The effect of spacecraft configuration will be more apparent when sampled structure does not vary too widely or is unimportant for the calculation of  $\nabla \cdot \boldsymbol{B}/|\nabla \times \boldsymbol{B}|$  and  $\delta J/|\boldsymbol{J}_{av}|$ , the latter being true when the spacecraft configuration scale is large relative to the model structure for instance (here Tsyganenko-87). Then the value of  $\nabla \cdot \boldsymbol{B}/|\nabla \times \boldsymbol{B}|$  is large, however, and the estimate of  $|\boldsymbol{J}_{av}|$  is unphysical  $(\delta J/|\boldsymbol{J}_{av}|$  can

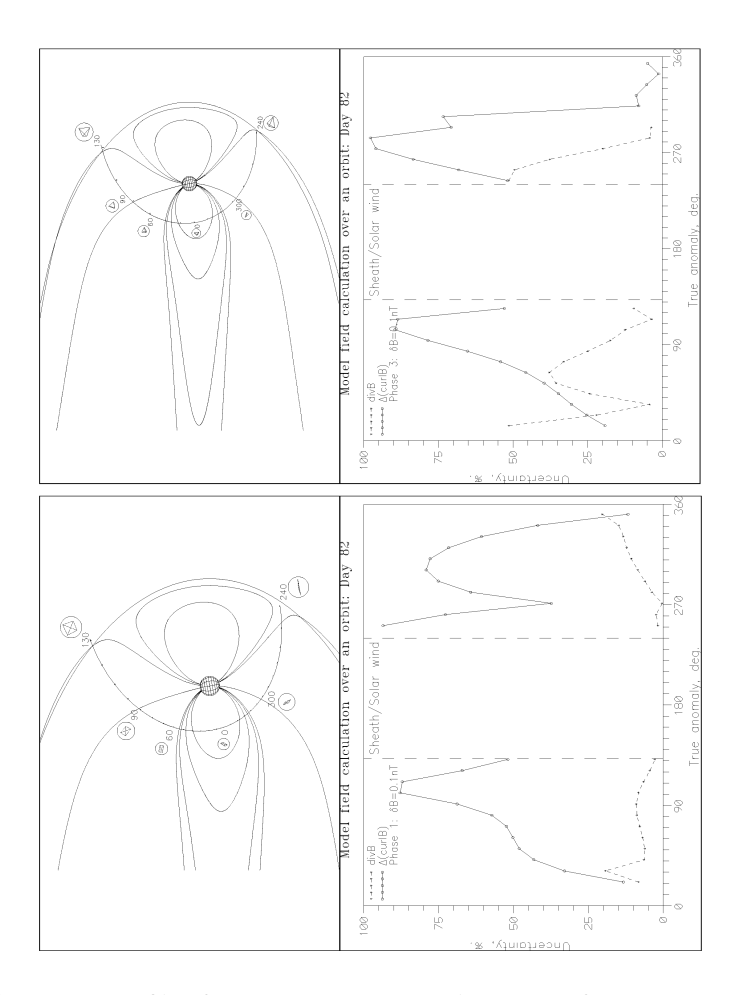


Figure 16.3: Error profiles for  $\nabla \cdot \boldsymbol{B}/|\nabla \times \boldsymbol{B}|$  and  $\delta J/|\boldsymbol{J}_{\rm av}|$  for two cases of dayside evolution, both with starting configurations at the northern cusp. The Tsyganenko model is used as model of magnetic structure.

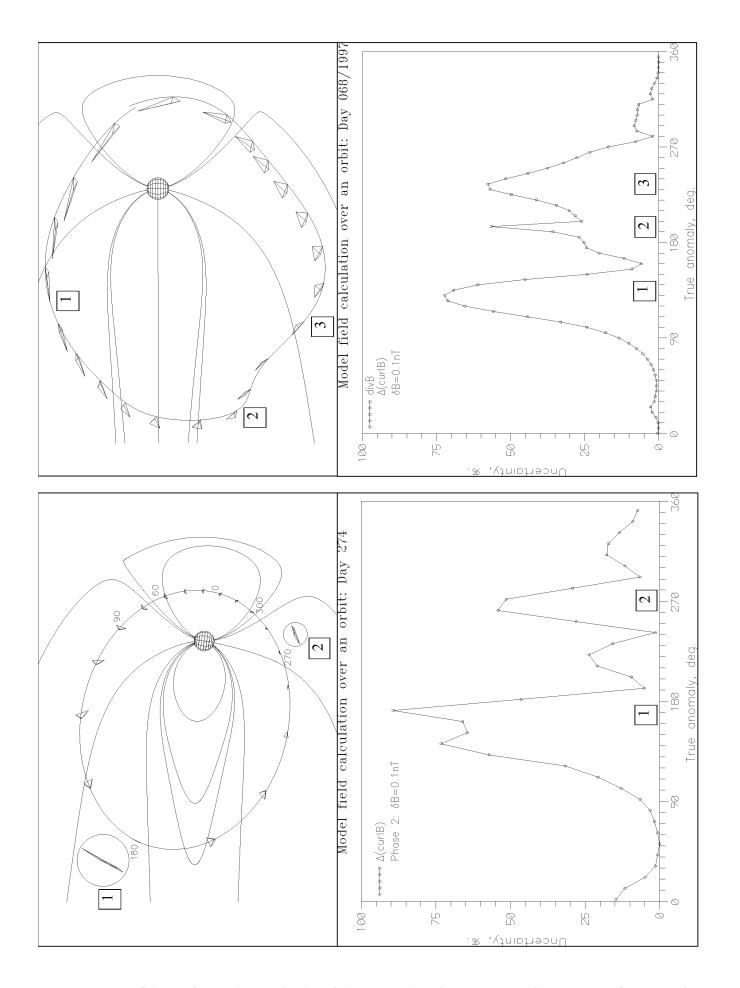


Figure 16.4: Error profiles for the nightside evolution, starting configuration at the magnetotail crossing (T87 model).

still be used as a quality estimate in this case).

In fact, in the context of the Cluster orbital configurations, it is only for the small separations shown in Figure 16.3 (<1000 km) that  $\nabla \cdot \boldsymbol{B}/|\nabla \times \boldsymbol{B}|$  remains small. Note that, because of the different evolution in each dayside case, the details of profile are different, but that, overall, the trends are similar, particularly the large deviation between  $\nabla \cdot \boldsymbol{B}/|\nabla \times \boldsymbol{B}|$  and  $\delta J/|\boldsymbol{J}_{av}|$ : the physical coverage remains good, but measurement error is bad as the spacecraft move away from the strong field region.

Key factors influencing the trends are the overall tetrahedral volume, the shape of the configuration, the magnitude of B and the nature of the field curvature. These factors combine to produce complicated dependencies and thus tetrahedral geometry alone is not a good indicator for predicting the errors in these cases. The consistent trend to large error in the plots for instance can be explained by the fact that the field magnitude varies considerably; falling dramatically as the magnetopause is approached. Generally, for small field intensities (and hence small differences between the spacecraft) the significance of the error is enhanced. For strong curvature in B the value of  $\nabla \cdot B / |\nabla \times B|$  may also grow. The peak at 30° in the left-hand plot, however, can be associated with extreme distortion in the tetrahedral shape. Similarly, the profiles after 240° are very different between the plots because the evolution is dramatically different (note that for the right-hand case the configuration is elongated in the direction perpendicular to the plane of view).

Figure 16.4 shows two cases for the nightside phase, for which a regular tetrahedron is set up close to the tail current sheet crossing. For these larger separations, while error quality is higher overall, reflecting the less critical nature of the separation error,  $\nabla \cdot \mathbf{B}$  is now large (not shown for clarity). The evolution for the left-hand plot shows two clear regions of severe distortion (as indicated by the insets, scaled by x10): one between  $120^{\circ}-180^{\circ}$  and one centred on  $270^{\circ}$ . These positions correspond to large errors in the current estimate. Moreover, the current density peaks through the current sheet so that  $\delta J/|\mathbf{J}_{av}|$  is suppressed. The right-hand plot shows the orbit plotted in GSM coordinates. While, clearly, the trends differ, in particular with regard to the positions of the peaks, the striking feature is perhaps the similarity in profiles. In the right-hand plot the current sheet is more clearly identified and the variation over the inner dayside magnetopause is smoother since the cusp structure is not well sampled. The error peaks are still clearly identified with extreme tetrahedral distortion, however; now with a double peak corresponding to the positions '2' and '3'.

Thus, for these large configurations, the effect of magnetic structure in  $\delta J/|\boldsymbol{J}_{\rm av}|$  has been reduced, so that  $F_S$  and  $F_B$  depend mainly on tetrahedral geometry. This is in contrast to the dayside phases where the effect of the sampled magnetic structure masks the effect of the tetrahedral geometry. The dependence of  $\nabla \cdot \boldsymbol{B}$  and  $\delta J/|\boldsymbol{J}_{\rm av}|$  on tetrahedral geometry is covered quantitatively in detail for specific model structure in the next section.

# 16.2.3 Analysis Technique

The preceding discussion has concentrated on issues most relating to the analysis of *in situ* data (for which there is no *a priori* knowledge of magnetic structure) and results in a conceptual method arising from the combined use of  $\nabla \cdot \mathbf{B}$  and  $\delta J/|\mathbf{J}_{av}|$  as quality monitors relating to the curlometer technique. The use of  $\nabla \cdot \mathbf{B}$  makes no distinction between those spatial gradients which contribute differently to  $\nabla \cdot \mathbf{B}$  and  $\nabla \times \mathbf{B}$ : there is an assumption that the terms in  $\nabla \cdot \mathbf{B}$ , as sampled, are as well represented, in combina-

tion, as the gradient terms in  $\nabla \times \boldsymbol{B}$ , or as poorly represented. The conceptual flow may contain further interpretation (or assumption) of event properties, however, following an initial analysis and combination of the data. This, of course, guides the application of the technique. The evidence obtained from simple models (e.g. where the direction of  $\nabla \times \boldsymbol{B}$  does not change) is that  $\nabla \cdot \boldsymbol{B}$  works well for indicating poor coverage for  $\boldsymbol{J}$ , at least in statistical sense. Such a technique has been designed and tested with a variety of simulated situations and is briefly described below.

Although an estimate for the current density can always be made, the above discussion suggests that two key areas of quality control can be pursued: the physical error, represented (crudely) by  $\nabla \cdot \boldsymbol{B}/|\nabla \times \boldsymbol{B}|$ , and the measurement error, represented by  $\delta J/|\boldsymbol{J}_{av}|$ . The estimate of  $\nabla \cdot \boldsymbol{B}$  itself separates the nature of the analysis which can be performed on actual events. Even if  $\nabla \cdot \boldsymbol{B}/|\nabla \times \boldsymbol{B}|$  is well behaved, measurement quality may not be high for all components of  $\boldsymbol{J}$ , and this must be monitored as part of the analysis. A poor estimate of  $\nabla \cdot \boldsymbol{B}/|\nabla \times \boldsymbol{B}|$  indicates a possibly poor physical estimate of some components of  $\boldsymbol{J}$ , requiring further (independent) interpretation of the sampled structure (for example, the size of the components of the gradient or stationarity properties). If  $\nabla \cdot \boldsymbol{B}/|\nabla \times \boldsymbol{B}|$  is not well behaved, therefore, gradient analysis can still be performed on individual terms in the dyadic  $\nabla \boldsymbol{B}$  and the time dependence of the event can be checked.

The technique has been used to investigate a number of simulated events using a variety of magnetic structures. It is clear from this study that for strongly anisotropic structures, having spatial scales at least of the order of the spatial scales of the spacecraft configuration, the orientation of the configuration with respect to model is crucial as suggested above. For some orientations the estimates show better coverage with distorted configurations than for regular configurations when comparing the estimated J to the mean current for the model.

# 16.3 Accuracy of Current Density Determination

## 16.3.1 Parameters Used to Define the Shape of a Tetrahedron

Chapter 13 is dedicated to the study of "quality factors" which could describe the shape of a tetrahedron. In the past, the relationship between the accuracy of the current density determination and the shape of the tetrahedron has been studied with various 1-D parameters. The main result was that there exist two categories of 1-D parameter: one which attempts to describe the geometrical shape, and a second which is directly connected to the relative accuracy of the measurement. This was a conclusion deduced from observation and simulation, but not explained. Chapter 13 studies this observation, and has checked the validity of the 1-D parameters. The main conclusion of that chapter is that the best way to describe the shape of the tetrahedron, and understand what happens, is to use a 2-D geometric factor, made up of two parameters, the *elongation E* and *planarity P* parameters, which are deduced from the volumetric tensor (see Chapters 12 and 13).

Here we take again this method, and all parameters such as the total difference between the estimated and the theoretical, mean |J| defined by the model,  $\Delta J/J$  (see precise definition in Section 16.3.5), and parameters such as  $\nabla \cdot \boldsymbol{B}$  and  $\nabla \times \boldsymbol{B}$  will be studied in an elongation-planarity (E-P) diagram, which allows us to characterise more precisely the relationship between the shape of the tetrahedron and the accuracy of the estimate of the

current density, and furthermore to understood why, in certain cases, the estimate of the measurement is good, and why, in other cases, this estimate is bad.

 $\Rightarrow$ 16.1

#### 16.3.2 Simulation Method

The following method has been used to check the possible relation between the shape of the tetrahedron and the accuracy of the current density determination:

- firstly, we use a high number of tetrahedra, corresponding to several possible geometric configurations, taken from a "configurations reservoir";
- secondly, we use a model of current density structure, with a characteristic scale larger than the size of the tetrahedron, such that all the vertices of the tetrahedron are contained inside the current structure;
- thirdly, we add independent noise on the B magnetic components at the 4 spacecraft positions (the four vertices of the tetrahedron) and we compute vector parameters such as  $\nabla \cdot B$ ,  $\nabla \times B$ , and the relative error  $\Delta J/J$  on the determination of J.

#### 16.3.3 The Tetrahedron Reservoir

The shape of the tetrahedron is characterised by the E-P parameter. We try to identify a possible relationship between the value of these parameters and the accuracy of the estimate of  $\nabla \times \boldsymbol{B}$  and  $\nabla \cdot \boldsymbol{B}$ . Firstly, to be sure that various kinds of tetrahedra are taken into account, we use the "homogeneous tetrahedra reservoir" defined in 13.5.1 of Chapter 13. This reservoir contains about 1000 tetrahedra and offers an homogeneous coverage of the E-P plane. So, this reservoir contains a wide variety of configurations. To avoid any bias, the tetrahedra taken from the reservoir are reprocessed as follows: (i) they are computed in the barycentric coordinates, (ii) all the tetrahedra are normalised to the same mean inter-spacecraft distance  $\langle D \rangle$ , (iii) their orientations are perturbed so as to have a random orientation in space, and (iv) the position of the centre of each tetrahedron is translated to  $-2500 \, \mathrm{km}$ , in order to avoid the centre of the current structure which could be a particular case.

#### **16.3.4** The Current Structure Models

The goal is to simulate the crossing of a current structure by the Cluster constellation. We have therefore to define a current structure model. The chosen model is described in Figures 16.5 and 16.6: it consists of a cylindrical current tube, with an homogeneous current density (Figure 16.5), or a Gaussian current density profile (Figure 16.6). In all cases, we assume that the size of the Cluster tetrahedron is smaller than the size of the current density structure, so that all the spacecraft are simultaneously located inside the current density structure. Typical values are  $\langle D \rangle = 1000 \, \mathrm{km}$ , R or  $\sigma = 5000 \, \mathrm{km}$ ,  $J_o = 10^{-8} \, \mathrm{amp/m^2}$ .

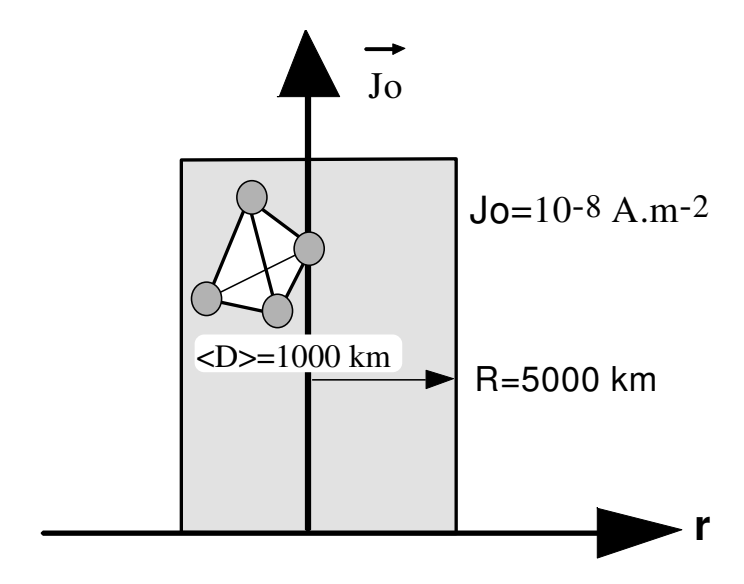


Figure 16.5: Current tube with homogeneous current density profile.

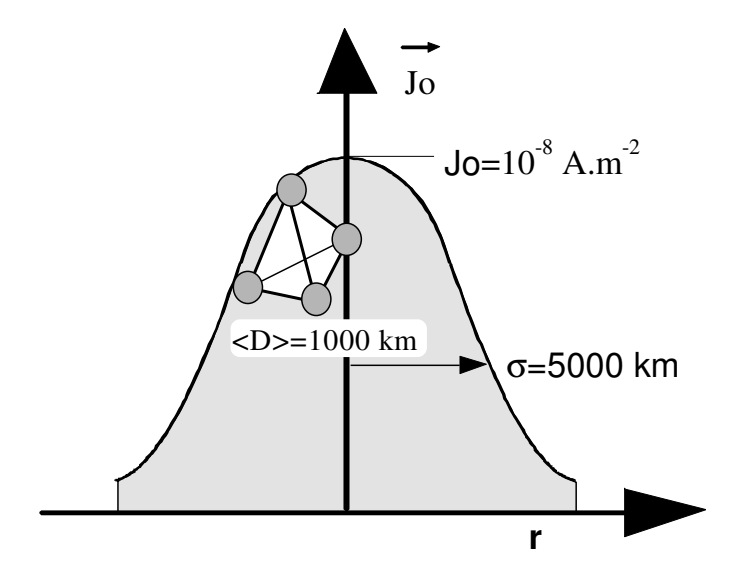


Figure 16.6: Current tube with Gaussian current density profile.

16.4. Results 407

# **16.3.5** The Computation of J and $\nabla \cdot B$

The uncertainty in the measurements of B (or the uncertainty in the restitution of the spacecraft attitude) is simulated by adding a random noise on the 3 components of the 4  $B_{\alpha}$  vectors. Similarly a random noise is added to the 4  $r_{\alpha}$  vectors describing the positions of the 4 spacecraft. The amplitude  $\Delta B$  of the noise added on the 4 magnetic field vectors is independent of the components, and proportional to |B|. The uncertainty  $\Delta r$  in the knowledge of the spacecraft position is taken to be proportional to  $\langle D \rangle$ , the average interspacecraft distance.  $\Delta B/B$  or  $\Delta r/r$  represent the relative accuracy in the determination of  $B_{\alpha}$  and  $r_{\alpha}$ . The relative errors  $\Delta B/B$  and  $\Delta r/r$  are defined as:

$$\Delta B/B = \Delta B/\frac{1}{N} \sum_{\alpha=1}^{4} |\boldsymbol{B}_{\alpha}|$$

$$\Delta r/r = \Delta r/\frac{1}{N} \sum_{\alpha=1}^{4} |\mathbf{r}_{\alpha}|$$

Typical values for  $\Delta r/r$  are 1%, which correspond to the nominal values given by the Cluster project.  $\nabla \cdot \mathbf{B}$  and  $\mathbf{J} = \nabla \times \mathbf{B}/\mu_0$  are computed from the perturbed simulated data by the barycentric coordinates method, and we obtain an estimate of the  $\mathbf{J}$  or  $\nabla \times \mathbf{B}/\mu_0$  vector which is compared to the real value of the average of  $\mathbf{J}$  at each vertex given by the model. Although the uncertainty in the modulus and the direction of  $\mathbf{J}$  have been studied, we present here only the results corresponding to the modulus of  $\mathbf{J}$ , that we note hereafter  $\mathbf{J}$ . Thus the relative accuracy of the estimate of  $\mathbf{J}$ ,  $\Delta \mathbf{J}/\mathbf{J}$ , can be estimated. The definition of  $\Delta \mathbf{J}/\mathbf{J}$  is:

$$\Delta J/J = \frac{\mu_0 \Delta J}{|\nabla \times \mathbf{\textit{B}}|^{\text{model}}} = \frac{|\mathbf{\textit{J}}^{\text{estimated}}| - |\mathbf{\textit{J}}^{\text{model}}|}{|\mathbf{\textit{I}}^{\text{model}}|}$$
(16.4)

where  $|J|^{\text{model}}|$  is the mean value of the  $4|J_i|$  values of the model at the 4 vertices of the tetrahedron, and  $|J|^{\text{estimated}}|$  is the estimate of |J| by the barycentric method, which is equivalent with  $|J|_{av}|$  used in Section 16.2. Of course, from Ampère's law, and taking into account the different kinds of errors, we note  $\mu_0|J|^{\text{estimated}}| = |\nabla \times B|^{\text{estimated}}|$ . It has been shown that the errors  $\Delta B/B$  or  $\Delta r/r$  have the same effect on the accuracy  $\Delta J/J$ . Therefore, for the sake of simplicity, we will only consider the perturbation  $\Delta r/r$ . This computation is made for all the tetrahedra taken from the reservoir defined in Chapter 13, thus all the E-P plane is covered.

# 16.4 Results

# 16.4.1 Influence of the Shape of the Tetrahedron on the Relative Accuracy $\Delta J/J$

First we consider an homogeneous current density profile, and therefore there is no error associated with the linear interpolation between the measurement made at the 4 spacecraft locations; only the uncertainties on the positions of the measurement points are taken into account  $(\Delta r/r = 1\%, \Delta B/B = 0)$ .

The main results are shown in Figure 16.7, where we have plotted the relative accuracy  $\Delta J/J$  in an E-P diagram. The size and the colours of the circles indicate the values of  $\Delta J/J$ : for  $\Delta J/J = 0$ , the radius of the circle is just an invisible point, the largest circles correspond to  $\Delta J/J \ge 10\%$ . Note that there is no small circle hidden behind a large one,  $\Rightarrow 16.2$ the circles being sorted by size before plotting.

 $\Rightarrow$ 16.3

Adopting the five types of tetrahedra defined in Chapter 13 as description of shape, the main conclusion is that for a large fraction of the diagram, corresponding to the "Pseudo-Spheres type" and to a large fraction of the "Potatoes type", the relative error  $\Delta J/J$  remains below 2%. For values of the elongation or planarity parameter larger than about 0.6, the errors reach 3% or more. For E or P > 0.9, which corresponds to a very long or a  $\Rightarrow 16.2$ very flat tetrahedron, the error can reach 10% and more, especially of course when both E and P get of the order of unity. As a matter of fact, the error increases roughly with the radius  $r = \sqrt{(E^2 + P^2)}$ , but this variation is not linear.

#### 16.4.2 Influence of the Shape of the Tetrahedron on the Estimate of $\nabla \cdot B/|\nabla \times B|$

Similar results are shown in the Figure 16.8, for  $\nabla \cdot \mathbf{B}$  and  $\nabla \times \mathbf{B}$  estimated from the simulated measurement values. Notice that the current density profile being homogeneous, the theoretical value of  $|\nabla \times \mathbf{B}|$  is the same for all the points, and the  $|\nabla \times \mathbf{B}|$  estimated values differs from the theoretical ones according the results of Figure 16.7 where  $\Delta J/J$ is defined by equation 16.4 (see Section 16.3.5).

The theoretical value of  $\nabla \cdot \mathbf{B}$  is obviously equal to zero. Since  $\nabla \cdot \mathbf{B}$  is not a normalised quantity, we have chosen to display the estimate of the ratio  $\nabla \cdot \mathbf{B}/|\nabla \times \mathbf{B}|$  rather than the value of  $\nabla \cdot \mathbf{B}$ . The colour code is the same as for  $\Delta J/J$ . Roughly speaking, the diagram looks the same as for  $\Delta J/J$ , the "Pseudo-Spheres" and "Potatoes" types gives the lower values of the divergence, and a large value of E or P leads to a large value of the estimated divergence.

#### 16.4.3 Relationship between $\Delta J/J$ and $\nabla \cdot B/|\nabla \times B|$

Since the  $\nabla \cdot \mathbf{B}/|\nabla \times \mathbf{B}|$  diagram looks the same as the  $\Delta J/J$  diagram, one would expect that the estimated ratio  $\nabla \cdot \mathbf{B}/|\nabla \times \mathbf{B}|$  is an estimate of the error  $\Delta J/J$ . This is statistically true (see previous section), but a more careful investigation shows that there is no one to one correspondence between the two diagrams; a large value of  $\Delta J/J$  can correspond to a small value of  $\nabla \cdot \mathbf{B}/|\nabla \times \mathbf{B}|$  ratio, and vice versa: good estimates of  $\mathbf{J}$ can correspond to large value of the divergence (large  $\nabla \cdot \mathbf{B} / |\nabla \times \mathbf{B}|$ ). This is particularly true for large values of E or P.

In order to reveal a possible relationship between  $\Delta J/J$  and  $\nabla \cdot \boldsymbol{B}/|\nabla \times \boldsymbol{B}|$ , we have plotted these quantities in together in Figure 16.9. The colour code and the symbols correspond to the family of the tetrahedra defined in Chapter 13 (circle for Pseudo-Spheres, horizontal ellipsoid for Cigars, triangle for Pancakes, diamond for Knife Blade, and oblique ellipsoid for Potatoes).

A possible relationship between these two parameter would result in the alignment of the representative points. This is not observed; the distribution of the points has no preferred direction. Of course the area of the "Pseudo-Spheres" (round symbols) is restricted to the central part of the diagram, close to zero, while the other types cover all the diagram.

16.4. Results 409

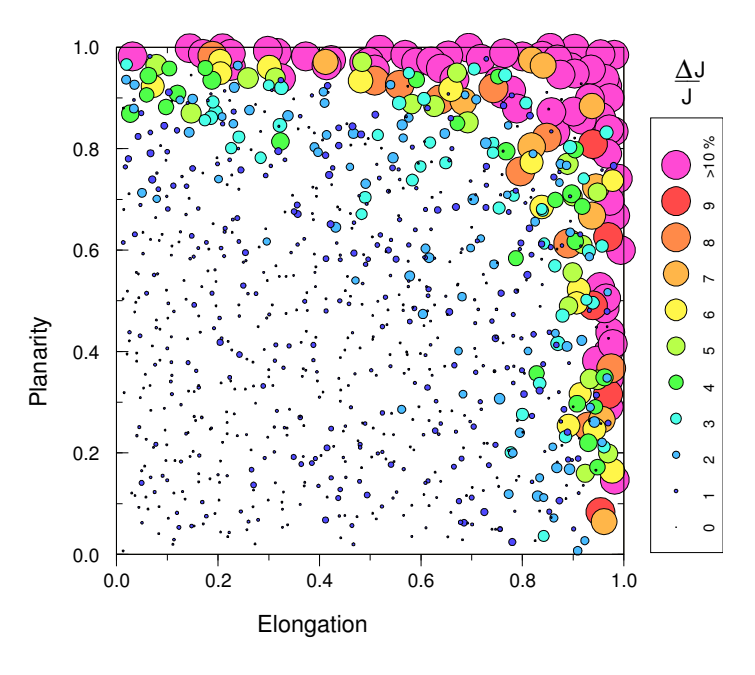


Figure 16.7: Influence of the shape of the tetrahedron on the estimate of |J|.

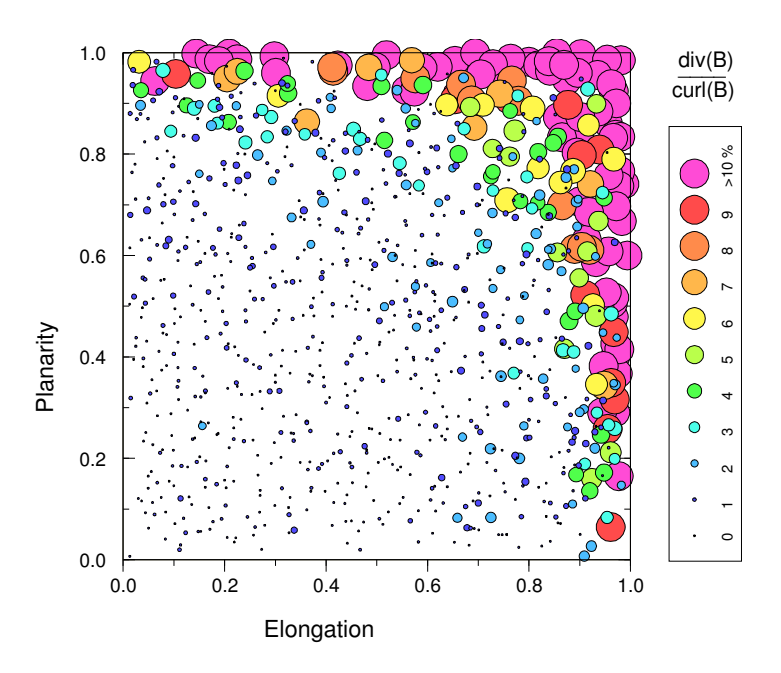


Figure 16.8: Influence of the shape of the tetrahedron on the estimate of the ratio  $\nabla \cdot \pmb{B}/|\nabla \times \pmb{B}|$ .

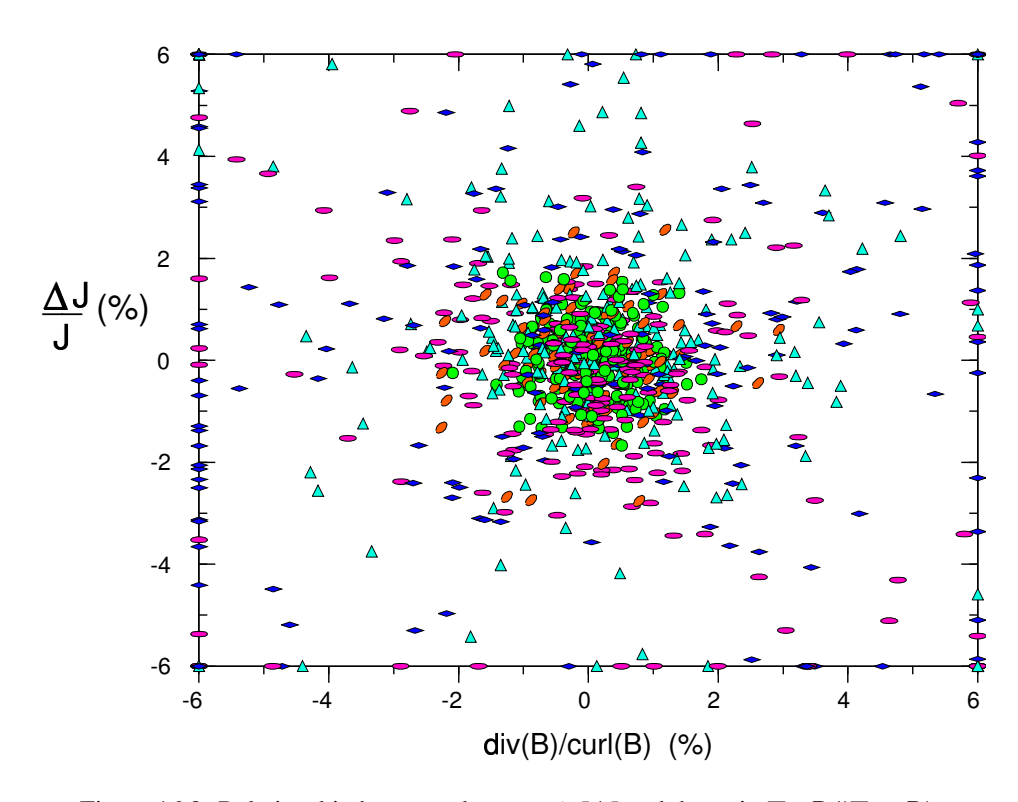


Figure 16.9: Relationship between the error  $\Delta J/J$  and the ratio  $\nabla \cdot \mathbf{B}/|\nabla \times \mathbf{B}|$ .

The non-existence of a correlation between  $\nabla \cdot \boldsymbol{B}$  and  $\Delta J$  can be explained by the fact that the computation of  $\nabla \cdot \boldsymbol{B}$  and  $\nabla \times \boldsymbol{B}$  involve different combinations of the components of the dyadic  $\nabla \boldsymbol{B}$ . The divergence is obtained from the diagonal terms, while the curl is built from the off-diagonal terms. These terms being perturbed by the addition of an independent random noise on the 12 components defining the 4 spacecraft positions to simulate the uncertainties on the measurement of these positions, the corresponding errors on the gradient tensor are not dependent. Practically, if the errors on the various components are effectively independent, it means that we cannot use the value of the estimated divergence to estimate the error  $\Delta J$  due to the measurement uncertainties. Thus, for sampling "blind events", the uncertainty on J can be calculated by equation 16.3 (see Section 16.2). Moreover, this result means that a particular configuration shape (classified by E-P) does not alone absolutely order the measurement error, except statistically (all orientations); the relative orientation to the magnetic structure also influences this (see Section 13.2 on "Measurement Performance", page 324).

# 16.4.4 Influence of the Current Direction on the Error $\Delta J/J$

In the present section, we investigate the possible influence of the direction of the current with respect to the largest face of the tetrahedron on the errors. Figure 16.10 shows the result: the relative error  $\Delta J/J$  is plotted versus the angle  $\theta$  between the direction of the current and the normal to the main plane of the tetrahedron. The main plane of the

16.4. Results 411

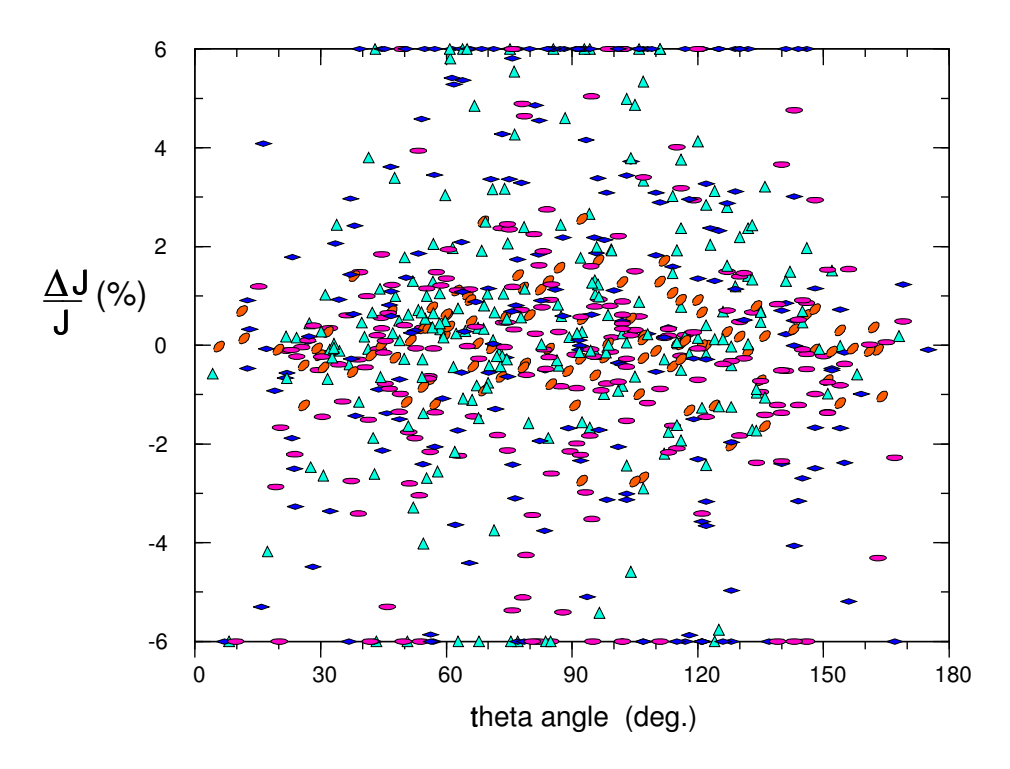


Figure 16.10: Influence of the current density direction on the error  $\Delta J/J$ .

tetrahedron is defined as the plane containing the major and middle semiaxes of the inertial ellipsoid, thus the normal to this plane is the minor semiaxis.

As defined in Section 16.4.3, a colour code and a symbol are used to separate the different families of tetrahedra defined in Chapter 13. The "Pseudo-Spheres" have been removed from the figure because the main plane has no meaning for a sphere. One could expect to find in this diagram a relationship between  $\Delta J/J$  and  $\theta$ , showing for instance that the quality of the estimate would be better when the current is orthogonal to the main plane. Examination of Figure 16.10 show that the (expected) minimum of  $\Delta J/J$  for  $\theta=0^\circ$  or  $\theta=180^\circ$  seems roughly clear. One can observe a slight tendency in the case of the "Pancakes", for which the main plane has of course the clearest meaning, but this relationship is not very obvious because the distribution of the point in this diagram is not homogeneous along the  $\theta$  axis, and there is not enough point near  $\theta=0^\circ$  or  $\theta=180^\circ$  to get a clear-cut conclusion. Therefore, practically, it seems that the angle  $\theta$  plays a role in the organisation of the diagram, and error  $\Delta J/J$  can be related to this angle, at least for the particular model of an homogeneous current tube.

# 16.4.5 Heterogeneous Current Profile

The estimate of the current density inside the volume defined by the tetrahedron relies on the assumption that the magnetic field varies linearly between two spacecraft. If the current density profile is not homogeneous in space (as it is the case here), higher orders derivatives introduce a key source of errors in the estimate of  $\nabla \times \boldsymbol{B}$  and  $\nabla \cdot \boldsymbol{B}$ . To study its effect, we use a Gaussian shape for the current density profile, such as the one shown in Figure 16.6, and define an heterogeneity factor  $h = \langle D \rangle / \sigma$  where  $\langle D \rangle$  is the mean inter-spacecraft distance and  $\sigma$  is the root mean square deviation of the Gaussian. In order to better illustrate the effect of heterogeneity of the profile, we hereafter neglect the uncertainties  $\Delta B/B$  and  $\Delta r/r$  which are set to zero.

Figure 16.11 shows the relationship between the shape of the tetrahedron, again defined by the E and P parameters, and the accuracy  $\Delta J/J$  of the estimate, for a low value of the heterogeneity factor.

The chosen value: h=0.1, being low, the profile of the current structure is not very heterogeneous at the scale of the Cluster tetrahedron, thus the relative error  $\Delta J/J$  is very low, except for large values of E or P. For large values of E and P we find a result similar to the homogeneous case (but then with a relative error  $\Delta r/r$  of 1%, see Figure 16.7 before). As before, the error grows up rapidly as soon as the tetrahedron degenerates to a very flat or a very elongated configuration. Increasing the heterogeneity factor, for instance h=0.2 (Figure 16.12), leads to a rapid growth of the error  $\Delta J/J$ , but the conclusion about the shape remains similar.

Nevertheless, it seems that the heterogeneous case is more sensitive to a flat or a linear tetrahedron than the homogeneous case; in other words it seems that the errors due to the linear interpolation are more sensitive for a non-regular tetrahedron that the errors associated with uncertainty on  $\Delta r/r$  or  $\Delta B/B$ . This is particularly true for the  $\nabla \cdot \boldsymbol{B}/|\nabla \times \boldsymbol{B}|$  ratio. Figures 16.13 and 16.14 show the ratio  $\nabla \cdot \boldsymbol{B}/|\nabla \times \boldsymbol{B}|$  for h=0.1 and h=0.2. Comparisons between Figures 16.13 and 16.14, and between Figures 16.11 and 16.12 show that  $\nabla \cdot \boldsymbol{B}/|\nabla \times \boldsymbol{B}|$  is more sensitive to the configuration than  $\Delta J/J$ . Since the errors on  $\nabla \cdot \boldsymbol{B}$  and  $|\nabla \times \boldsymbol{B}|$  are unrelated, the total error on the  $\nabla \cdot \boldsymbol{B}/|\nabla \times \boldsymbol{B}|$  ratio is larger (no closely quantitative correspondence is anyway implied).

We have checked that the other conclusions, obtained in the homogeneous case, remain the same in the heterogeneous case. In particular, Figures 16.9 and 16.10 look the same with a finite low value of h. Thus, even in the heterogeneous case, there is no point to point correlation between  $\Delta J/J$  and  $\nabla \cdot \boldsymbol{B}/|\nabla \times \boldsymbol{B}|$ . The relationship between  $\Delta J/J$  and the angle  $\theta$  is apparent, particularly near the limiting values  $\theta = 0^{\circ}$  or  $\theta = 180^{\circ}$ , with the same restriction than the one for the homogeneous case.

#### 16.5 Conclusions

The curlometer technique, for in situ measurements, uses two parameters to monitor different quality aspects:  $\nabla \cdot \boldsymbol{B}/|\nabla \times \boldsymbol{B}|$  and  $\delta J/|\boldsymbol{J}_{av}|$ . A large value of  $\nabla \cdot \boldsymbol{B}$ , due to nonlinear dependence in the gradients contributing to  $\nabla \cdot \boldsymbol{B}$  (assuming that the measurement errors are weak regarding the physical error), may indicate that  $\boldsymbol{J}$  is badly represented by the data, unless the sampling is favourable. The sampling achieved arises from both the configuration parameters (including relative orientation and scale) and the particular magnetic structure encountered (which defines the character of terms in the gradients matrix of  $\boldsymbol{B}$ ). But, of course, when handling real data, we have to assume that  $\boldsymbol{J}$  will be badly measured, as indicated by  $\nabla \cdot \boldsymbol{B}$ , until we know otherwise. In this regard, other analysis techniques or model assumptions, which need to be checked for consistency, may be used iteratively with the curlometer to improve understanding of an event. When  $\nabla \cdot \boldsymbol{B}$  is small,

16.5. Conclusions 413

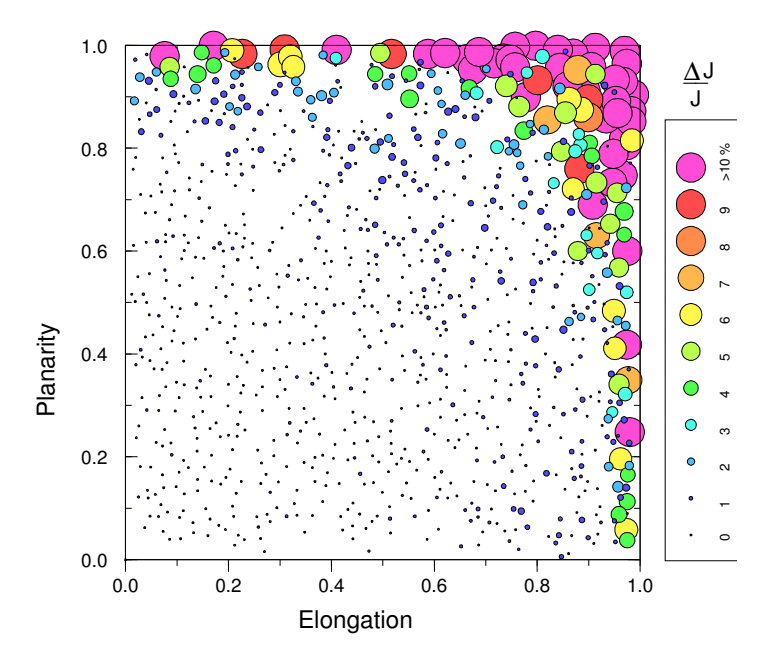


Figure 16.11: Influence of the shape of the tetrahedron on the estimate of J for a low degree of heterogeneity (h = 0.1).

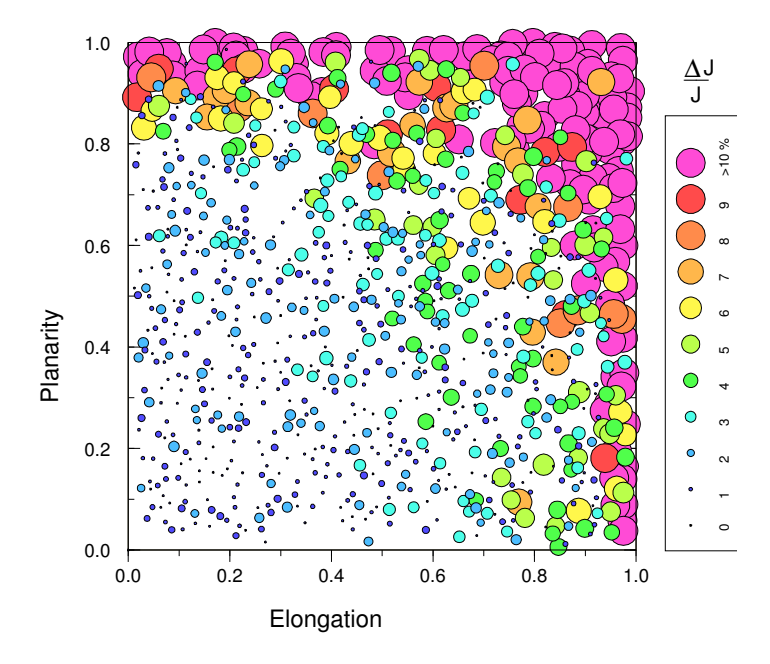


Figure 16.12: Same as Figure 16.11, but for a higher degree of heterogeneity (h = 0.2).

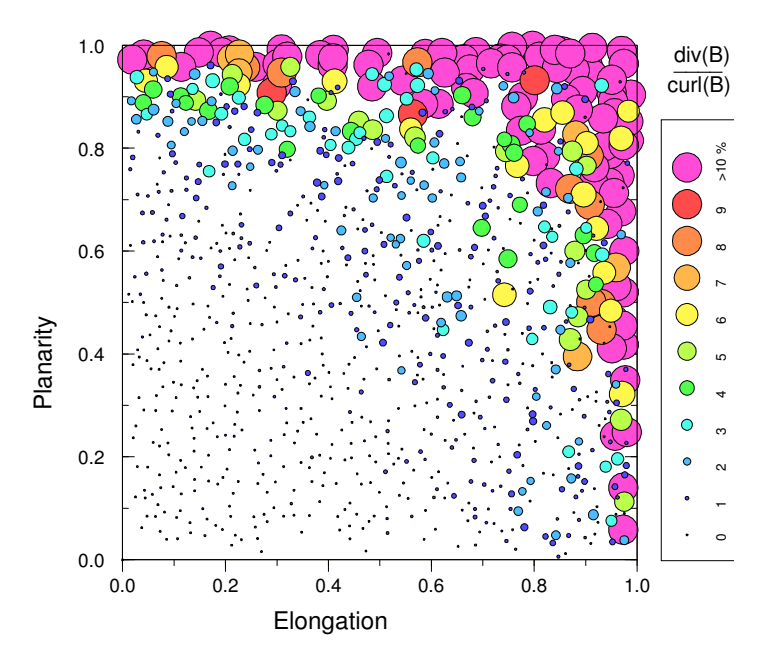


Figure 16.13: Influence of the shape of the tetrahedron on the estimated ratio  $\nabla \cdot \boldsymbol{B}/|\nabla \times \boldsymbol{B}|$ , for a low degree of heterogeneity  $(h=0.1, \Delta B/B=\Delta r/r=0)$ .

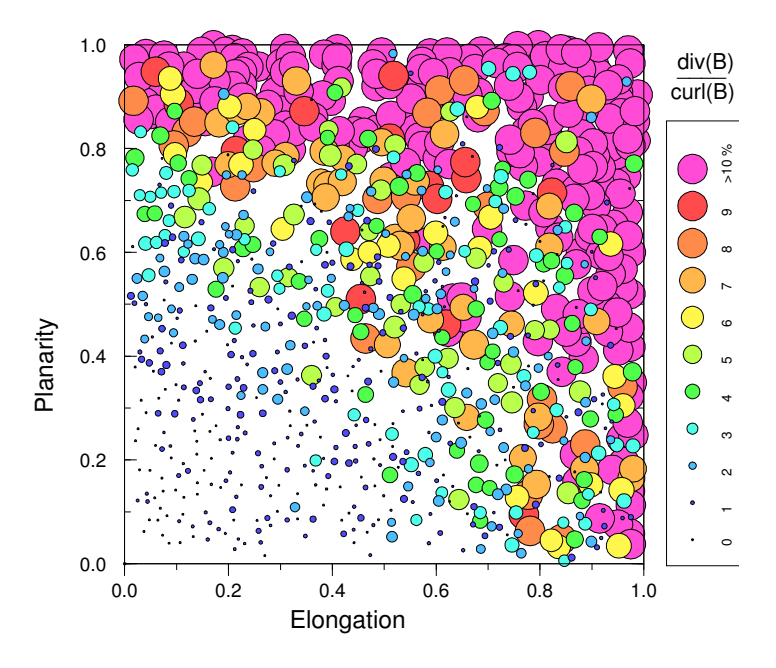


Figure 16.14: Same as Figure 16.13, but for a higher degree of heterogeneity (h=0.2).

16.5. Conclusions 415

we can assume that J remains statistically (and statistically only, see below the conclusion about the relationship between  $\nabla \cdot \boldsymbol{B}$  and  $\delta J$ ) well represented by the data unless the measurement error contribution  $\delta J/|\boldsymbol{J}_{av}|$  (coming from  $\delta B$  and  $\delta r$ ), to the error in  $\boldsymbol{J}$ , is large.

We therefore have two nearly independent parameters for the *in situ* monitoring:  $\nabla \cdot \mathbf{B}$  which may indicates a physical sampling error when the nonlinear terms dominate, and  $\delta J/|\mathbf{J}_{av}|$  which identifies measurement accuracy. It should be understood that not all situations are conducive to the technique and full analysis is performed by hierarchical application of a number of different techniques.

A significant result from Section 16.2 is that  $\nabla \cdot \boldsymbol{B}$  is large for the Cluster orbit phases given, where the Cluster tetrahedron is moving into the Tsyganenko-87 magnetic field model. The parameter  $\delta j/|\boldsymbol{J}_{av}|$  is smaller, overall, for the larger separations. This is more or less as expected:  $\boldsymbol{J}$  is physically better represented by the data when the tetrahedral dimensions are small, but  $\delta j/|\boldsymbol{J}_{av}|$  is smaller for large configurations, due to the combined effects of larger field differences between the satellites and a small ( $\sim$ 1%) relative error in the separations. For the mission phases considered here, an optimum range of separation scales, where both the physical estimate and the measurement accuracy remain good, does not exist. The parameters show several instances where the physical coverage (roughly represented by  $\nabla \cdot \boldsymbol{B}$ ) is insufficient to identify overall quality for the measurement.

To characterise the shape of the tetrahedron, as we have seen in Chapter 12 and 13, the best way is to use the elongation and planarity parameters (E, P) defined and used in Chapter 13 for the description of the shape. Its orientation in space is defined by the three orthogonal vectors corresponding to the directions of the three axes of the pseudo-ellipsoid computed from the volumetric tensor defined in Chapter 12. Vector c corresponds to the minor axis and is used for description of the orientation of the main face. By introducing the E-P diagram to plot quantities such as the relative accuracy  $\Delta J/J$  or other interesting quantities, we have a good tool to analyse the relationship between a scientific parameter and the shape of the tetrahedron, for a given event model. In the same manner, by using the  $\theta$  angle between the c vector and the direction of the current, we can analyse the effect of the orientation of the tetrahedron on the accuracy of the measurement.

The relationship between the shape of the tetrahedron and  $\Delta J/J$  has been shown by a simulation of the crossing, by 4 spacecraft, of a particular current density structure. This simulation allows an independent estimate of the effects of the various error sources, such as uncertainties on the position of the spacecraft, on the magnetometer measurements, and errors due to the spatial interpolation used for the computation of the various vector gradients. The simulation gives the relative accuracy  $\Delta J/J$  of the measurement for all variables. In particular, the accuracy  $\Delta J/J$  has been plotted in an (E-P) diagram, which organises the results well and relates easily the shape of the tetrahedron to the accuracy of the estimate of J or  $\nabla \cdot B$ . Furthermore, the E-P diagram is useful to get a quantitative estimate of this influence, and to check whether a regular tetrahedron leads to a more accurate estimate of J and  $\nabla \cdot B$  than the corresponding estimates for a distorted tetrahedron. Roughly speaking, the distance between the representative point and the origin is proportional to the error on the accuracy of the estimate of both these quantities which, statistically only, show the same trend (see below).

The conclusions are roughly the same for homogeneous and for heterogeneous cases, but it seems that the error due to linear interpolation, in the heterogeneous case, is more

sensitive to a non-regular tetrahedron than the errors due to a relative uncertainty  $\Delta r/r$  on the positions. This is particularly true for the  $\nabla \cdot \boldsymbol{B}/|\nabla \times \boldsymbol{B}|$  ratio. In a future work, it would be interesting to quantify the amplitude of the linearity errors versus the heterogeneity parameter.

A potential relationship between  $\nabla \cdot \mathbf{B}$  and  $\Delta J$  has been studied in detail. Statistically, the ratio  $\nabla \cdot \mathbf{B}/|\nabla \times \mathbf{B}|$  has the same behaviour as  $\Delta J/J$ , but on close inspection there is no one to one correspondence. There are at least two reasons for this. Firstly, one reason is obvious: since  $\nabla \cdot \mathbf{B}$  and  $\nabla \times \mathbf{B}$  are computed from different terms of the dyadic  $\nabla \mathbf{B}$  used by the barycentric method (see Chapters 14 and 15), and unless the errors are dependent (this can be nevertheless the case for special structures), there is no point to point correlation between the estimated  $\nabla \cdot \mathbf{B}$  and the estimated  $\nabla \times \mathbf{B}$  and therefore no correlation between  $\nabla \cdot \mathbf{B}/|\nabla \times \mathbf{B}|$  and  $\Delta J/J$ . A second additional reason is that the orientation of the tetrahedron in particular cases, associated with the particular current density structure used, plays a controlling role in this lack of correspondence which has to be more explained. Thus, if the various contributions to measurement errors are independent or if the nonlinear contributions to  $\nabla \cdot \mathbf{B}$  and  $\nabla \times \mathbf{B}$  are independent, then  $\nabla \cdot \mathbf{B}$  should not be used as a reliable estimate of the overall accuracy of the measurement of J. Nevertheless, for straight current tubes, the statistical behaviour of  $\nabla \cdot \mathbf{B}/|\nabla \times \mathbf{B}|$  looks the same as  $\Delta J/J$ , which gives justification of the use of  $\nabla \cdot \mathbf{B}$  as an indication of the quality of the physical coverage if the measurement errors can be neglected, or of the measurement error if the current structure is homogeneous.

The influence of the direction of the current with respect to the orientation of the tetrahedron has been examined. Indeed, for a nearly flat tetrahedron, one would expect a relationship between the angle  $\theta$  (defined as the angle between the direction of the current and the normal to the main plane of the tetrahedron) and the  $\Delta J/J$  error. The simulation shows that a relation exists, but the low number of points near  $\theta$  close to  $0^{\circ}$  or  $180^{\circ}$  leads to a reserved conclusion. Other simulations are necessary to better clarify this relation, and in particular to identify the behaviour in this context of the different type of tetrahedra such as Pancakes, Knife Blades, Cigars, etc.

All these conclusions, of course, could be modified for another type of magnetic structure. The effect of different characteristic magnetic properties (events sampled) on measurement performance needs to be investigated more thoroughly, particularly with regard to anisotropic structure. Tools and simulations used in this chapter are well suited for such an event study and should be performed in conjunction with other possible methods.

# **Bibliography**

The three methods for combining multipoint magnetometer data and their associated errors were discussed by:

Dunlop, M. W., Southwood, D. J., Glassmeier, K.-H., and Neubauer, F. M., Analysis of multipoint magnetometer data, Adv. Space Res., 8, (9)273–(9)277, 1988.

Dunlop, M. W., Balogh, A., Southwood, D. J., Elphic, R. C., Glassmeier, K.-H., and Neubauer, F. M., Configurational sensitivity of multipoint magnetic field measurements, in *Proceedings of the International Workshop on "Space Plasma Physics Investigations*"

16.5. Conclusions 417

by Cluster and Regatta", Graz, Feb. 20–22,1990, ESA SP–306, pp. 23–28, European Space Agency, Paris, France, 1990.

- Robert, P. and Roux, A., Accuracy of the estimate of J via multipoint measurements, in *Proceedings of the International Workshop on "Space Plasma Physics Investigations by Cluster and Regatta"*, *Graz, Feb. 20–22,1990*, ESA SP–306, pp. 29–35, European Space Agency, Paris, France, 1990.
- Barycentric coordinates were first applied to derivation of  $\nabla \times \mathbf{B}$  by:
- Chanteur, G. and Mottez, F., Geometrical tools for Cluster data analysis, in *Proc. International Conf. "Spatio-Temporal Analysis for Resolving plasma Turbulence (START)"*, *Aussois, 31 Jan.–5 Feb. 1993*, ESA WPP–047, pp. 341–344, European Space Agency, Paris, France, 1993.
- The dependence of the accuracy of J or  $\nabla \times B$  was evaluated by:
- Coeur-Joly, O., Robert, P., Chanteur, G., and Roux, A., Simulated daily summaries of Cluster four-point magnetic field measurements, in *Proceedings of Cluster Workshops, Braunschweig, 28–30 Sep. 1994, Toulouse, 16–17 Nov. 1994*, ESA SP–371, pp. 223–227, European Space Agency, Paris, France, 1995.
- Dunlop, M. W. and Balogh, A., On the analysis and interpretation of four spacecraft magnetic field measurements in terms of small scale plasma processes, in *Proc. International Conf. "Spatio-Temporal Analysis for Resolving plasma Turbulence (START)"*, *Aussois, 31 Jan.*–5 *Feb. 1993*, ESA WPP–047, pp. 223–228, European Space Agency, Paris, France, 1993.
- Dunlop, M. W., Southwood, D. J., and Balogh, A., The Cluster configuration and the directional dependence of coherence lengths in the magnetosheath, in *Proc. International Conf. "Spatio-Temporal Analysis for Resolving plasma Turbulence (START)"*, *Aussois, 31 Jan.–5 Feb. 1993*, ESA WPP–047, pp. 295–299, European Space Agency, Paris, France, 1993.
- Robert, P. and Roux, A., Influence of the shape of the tetrahedron on the accuracy of the estimation of the current density, in *Proc. International Conf. "Spatio-Temporal Analysis for Resolving plasma Turbulence (START)"*, *Aussois, 31 Jan.–5 Feb. 1993*, ESA WPP–047, pp. 289–293, European Space Agency, Paris, France, 1993.
- Robert, P., Roux, A., and Coeur-Joly, O., Validity of the estimate of the current density along Cluster orbit with simulated magnetic data, in *Proceedings of Cluster Workshops, Braunschweig, 28–30 Sep. 1994, Toulouse, 16–17 Nov. 1994*, ESA SP–371, pp. 229–233, European Space Agency, Paris, France, 1995.
- Robert, P., Roux, A., and Chanteur, G., Accuracy of the determination of the current density via four satellites, in *Abstracts*, International Union of Geodesy and Geophysics, XXI General Assembly, Boulder, Colorado, 1995, presentation GAB51H-06.
- The Tsyganenko-87 magnetic field model has been used to test the applicability of the proposed techniques:
- Tsyganenko, N. A., Global quantitative models of the geomagnetic field in the cis-lunar magnetosphere for different disturbance levels, *Planet. Space Sci.*, **35**, 1347–1359, 1987.
- The FGM magnetometer instrument on board Cluster is described by:

Balogh, A., Dunlop, M. W., Cowley, S. W. H., Southwood, D. J., Thomlinson, J. G., Glassmeier, K.-H., Musmann, G., Luhr, H., Buchert, S., Acuna, M., Fairfield, D. H., Slavin, J. A., Riedler, W., Schwingenschuh, K., and Kivelson, M. G., The Cluster magnetic field investigation, *Space Sci. Rev.*, 79, 65–91, 1997.